Acoustic Microscopy of Portland Cement Mortar Aggregate/Paste Interfaces

M. PRASAD[*], M. H. MANGHNANI, Y. WANG, P. ZININ,
School of Ocean and Earth Science and Technology
University of Hawaii, Honolulu, HI 9682, USA

R.A. LIVINGSTON
Federal Highway Administration
Turner-Fairbank Highway Research Center, McLean, VA 22101, USA

3 December, 1999

[*] Now at SRB Project, Geophysics Department,
Stanford University, Stanford, CA 94305

ABSTRACT

We have demonstrated the use of acoustic microscopy to characterize hydrated Portland cement microstructure. High frequency (1 GHz) studies identified reaction zones around bubbles, ettringite formation, and effects of aggregate composition. Lower frequency images (200-400 MHz) have been used to characterize effects of aggregate composition on cement/grain interface. The information obtained from acoustic microscopy complements optical and scanning electron microscopy. We demonstrate the importance of acoustic microscopy as an important nondestructive in situ technique for characterization of concrete. A major, unique advantage of the scanning acoustic microscope technique is its capability of penetrating into the material, which allows us to study cracks, defects and other zones of weakness that might be hidden below the surface.

Keywords: Concrete, Acoustic microscopy, microstructure, nondestructive testing.

1. Introduction

Portland cement concrete is one of the most commonly used man-made materials. Its mechanical strength and durability are functions of the various chemical processes occurring during the mixing and curing processes [1]. A major factor determining the strength of the concrete is the bond at the interface of the matrix and the aggregates [2]. The interfacial zones between the cement paste and aggregates are considered to be about 25 – 70 μm thick and are characterized by high porosity and abundance of hydrated crystalline products such as portlandite and ettringite [3]. They form the weakest part in the concrete structure where cracks can propagate more easily [3,4]. Microstructural and micromechanical characterization of these interfaces yields important insight in the development of the concrete properties, in particular their degradation with time. It is also invaluable in devising techniques to improve the strength and durability of concrete.

Recently, it has been shown that scanning acoustic microscopy (SAM) can provide additional information [5,6] that complements classical methods of interface characterisation, such as optical microscopy [3,7] and scanning electron microscopy (SEM) [3,8]. Acoustic waves can propagate through optically opaque materials, which makes acoustic mapping an important tool for *in situ* characterisation of elastic and strength properties of concrete. Micro-and macrostructural variations in the elastic properties can be imaged using acoustic waves at different frequencies. Since the wave propagation is extremely sensitive to local variations in elastic properties (elastic moduli and density), this technique is ideally suited for characterizing the interfacial and microstructural properties of concrete. Most studies of the mechanical structure of concrete have been done in the low (MHz) frequency range [9,10,11]. In this range only the large voids or cracks (several centimeters) can be studied. In order to detect features that might be associated with degradation, the elastic properties should be mapped at a micrometer scale, that is, at the scale of the transition zone between the cement and aggregates, which is responsible for the deterioration of concrete [2]. A preliminary study conducted with a high frequency (0.8 –2 GHz)

microscope on a Portland cement mortar with granitic aggregates [6] demonstrated for the first time that the mechanical structure of interfaces between cement matrix and aggregate can be examined with the desired micron resolution.

In this paper we study the interfaces between aggregates and paste, bubble and paste using acoustic microscopy. We describe applications of SAM to the following relevant problems on concrete characterizations: acoustical contrast of the aggregate and cement matrix interfaces, visualization of the subsurface interfaces, imaging of structure within the cement matrix and imaging of the ettringite formation. We present representative acoustic images of these features along with scanning electron microscopy (SEM) and reflected-light optical microscopy images to support the results. A complete interpretation of obtained results has been made by combining high and low-frequency acoustic microscopy, SEM, reflected-light optical microscopy and energy dispersive (X-Ray) spectroscopy (EDS).

2. Experimental Method

The high frequency acoustic microscope with a spatial resolution of about 1 μm is the acoustic equivalent of an optical microscope [12]. In the acoustic microscope a monochromatic acoustical signal is focused onto the specimen through the sapphire rod and the couplant (usually water) between the lens and the sample. Acoustic images are obtained when the acoustic microscope mechanically scans the sample in a plane parallel to the sample surface. Variation of the mechanical properties with depth can be studied by scanning the sample at various lens positions. The acoustic wave propagates through the coupling fluid to the sample surface and is reflected by the surface of the sample with the reflectance function $R(\theta)$. When the acoustic wave are defocused into the sample by a distance z, they experience a phase delay of $2z\,k\cos\theta$. The total output signal $V(z)$ received at the transducer is a function of the depth of defocus z and is calculated by integrating the wavefront over the surface of the transducer. Assuming

that the material is isotropic and that the transfer function of the lens is independent from the azimutal angle, [13,14]

$$V(z) = \int_0^{\alpha} P(\theta) R(\theta) e^{-i2zk\cos\theta} \sin\theta \cos\theta d\theta \quad , \qquad (1)$$

where α is the half-aperture of the lens, k is wave number, $P(\theta)$ is the combined pupil function [12], and $R(\theta)$ is the reflection coefficient [15]

$$R(\theta) = \frac{Z_{tot} - Z_W}{Z_{tot} + Z_W}. \qquad (2)$$

Here Z are the acoustic impedances defined by

$$Z_L = \frac{\rho_S v_L}{\cos\theta_L}, Z_T = \frac{\rho_S v_T}{\cos\theta_T}, Z_W = \frac{\rho_W v_W}{\cos\theta}, Z_{tot} = Z_L \cos^2(2\theta_T) + Z_T \cos^2(2\theta_T), \qquad (3)$$

and where ρ_S , v_L, v_T are respectively the density, longitudinal wave velocity and shear wave velocity of the specimen; and ρ_W , v_W are respectively the density and the longitudinal wave velocity of water. Angles θ_L and θ_T are determined from relations

$$\sin\theta_L = \frac{v_W}{v_L}, \sin\theta_T = \frac{v_W}{v_T}. \qquad (4)$$

As can be seen from (1), contrast in the acoustic microscope represents the variation of the acoustical properties of the sample and is dependent of the defocusing distance z. Penetrating power of the acoustic waves into the specimen is a function of the frequency of the acoustic waves. Low frequency waves penetrate deeper into the material. In the present study we used an Ernst Leitz scanning acoustic microscope (ELSAM) with a high frequency lens (about 1 GHz) to investigate fine structure of the interfaces and low frequency lenses (100 MHz – 400 MHz) to investigate deep structures in concrete.

3. Sample preparation

Concrete samples investigated in this study were prepared by casting plain cement paste or silica fume paste with different types of aggregates (andesite, granite). Detailed description of the samples can be found elsewhere [8]. One sample used in this study was obtained from a failed concrete block, presumably due to ettringite formation. This sample was investigated to identify ettringite formation.

To obtain a high quality acoustic image at high (GHz) frequency range, the surface of the sample must be polished to make roughness smaller than 1/10 microns. The concrete samples were embedded in epoxy resin, ground on each side, and then polished to a final finish of 0.1 μm. The two sides were parallel to about 1.0 μm. Due to variable stiffness of the cement matrix and aggregates, polishing required special care in order to prevent topographic effects between grains and matrix.

4. Results and discussion

4.1 Aggregate and Cement Matrix Interfaces

The contact zone between aggregate and cement paste is of major interest in concrete characterization because this zone forms a weak link in concrete where cracks can easily develop. Usually aggregates are considered as inert parts in the concrete formation [3]. Recently, Uchikawa [7] has shown that the aggregate type and its surface structure play an important role in determining the properties of the contact zone. Analysis of high frequency acoustical micrographs demonstrates that different aggregate compositions produce different microstructures of the contact zone. Fig. 1 shows acoustic and SEM images of a granitic aggregate in cement matrix. The various mineral compositions were identified by EDS analyses.

The acoustic image in Fig. 1 demonstrates various types of aggregate grain boundaries with the matrix. The quartz, and to some extent plagioclase, grains have sharp and well defined grain boundaries. The smooth boundaries of the quartz and plagioclase grains imply chemical inertness of the aggregates.

In contrast the boundaries of both the albite and hornblende grains are very irregular. The frayed boundaries of the albite grain suggest extensive chemical reactions between the grain and the cement matrix. The hornblende grain has almost completely reacted. The relative reactivity of the minerals appears to follow the trends observed in metamorphic petrology. Amphiboles, i.e., hornblende, would be the farthest from equilibrium with an aqueous solution. At Earth surface conditions, a highly alkaline solution typical of concrete pore solutions would be most reactive and would react with hornblende first. In contrast, quartz would be the closest to equilibrium and the feldspars would be intermediate. Note that the calcium rich plagioclase shows less reactivity with the calcium-containing matrix than with the sodium-rich albite. Fig. 2 also shows some gel at the lower end of the quartz grain. This gel does not appear to have been derived from the quartz, but possibly from some other unidentified grain that is not located in the plane of this image. A complex microstructure can be seen in the cement paste regions (Fig. 1), reflecting local variations in the amounts of crystalline calcium hydroxide and amorphous C-S-H. This could provide the basis for a quantitative estimate of the ratio of calcium hydroxide to C-S-H

Fig. 2 shows the cement paste-aggregate interaction for another type of aggregate in this case, andesite. This igneous rock has a chemical composition similar to granite. However, it is of volcanic origin and as a result, does not have the well developed crystalline structure. The fine-grained andesite would be likely to be more reactive. The effect of reaction on the aggregate boundaries is clearly seen in Fig.2. There are finger-like growths along the edges, which continue into the cement paste.

4.2. Imaging of Subsurface Interfaces

One of the unique features of the acoustic microscopy is the ability to visualize subsurface microstructures not observed by optical microscopy [14, 20]. A comparison of acoustic, reflected-light, and scanning electron microscopy images of a cement mortar specimen with andesitic aggregates and silica fume is shown in Figs. 3 and 4. Acoustic micrographs made at 200 MHz and at 400 MHz are

presented in Figs. 3a and 3b, respectively. Since the attenuation of sound is very high at 1 GHz, images of subsurface interfaces (e.g., Fig. 3b at defocus z = -100 μm) were taken only at a low frequency of 200 MHz. A better resolution image of the aggregate surface was made at higher (400 MHz) frequency (Fig. 3a). In all four images (acoustic in Fig. 3, optical and SEM in Fig 4) made of the same area, the bubble structure is seen clearly on the right hand side. Surface (Fig. 3a) and subsurface (Fig. 3b) images of aggregate exhibit excellent contrast of aggregate boundaries. As defocus increases, the boundary of aggregate appears closer to the bubble (Fig. 3b). Numerous black spots, most likely representative of voids, are observed in the surface acoustic image in Fig. 3a. They hamper investigations of the interfaces within concrete, when the acoustic waves are focussed at the surface. These effects can be eliminated by defocusing the acoustic waves below the surface as shown in Fig. 3b. The reflected-light optical and SEM images (Figs. 4a and 4b, respectively) are quite distinct from the acoustic images. Aggregate boundaries are only faintly visible in the SEM images and not seen at all in the optical images. Furthermore, the SEM image shows numerous cracks. These cracks are formed typically in samples, which have not been fully cured. During SEM, the high vacuum leads to water evaporation from the matrix. This water evaporation from the sample causes a change in volume of the paste and leads to formation of cracks. Such cracks were observed in most SEM investigations performed during this study. These comparative examples of acoustic, reflected-light optical and scanning electron microscopy demonstrate the strength of SAM over the traditional methods of microstructural characterizations.

4.3. Bubble and Cement Matrix Interfaces

Voids are typical features found in cement pastes. A long standing question in concrete technology is the nature of the bubble/matrix interface. 400 MHz SAM and SEM images of a bubble structure in cement paste are shown in Figs. 5a and 5b, respectively. Under the scanning electron microscope, a relatively broad reaction rim can barely be seen (Fig. 5b). In the SAM image, a thin layer

is revealed within the reaction rim. Below the Rayleigh angle the brightness of contrast of the SAM image in focus (see equations (1)-(2)) is mainly determined by difference between impedances of liquid and of solid. High contrast of the layer around the bubble indicates a high impedance and hence a relatively high hardness. As mentioned earlier, SEM images showed numerous major cracks in the sample.

4.4. Ettringite Formation

Formation and presence of ettringite in hardened concrete is often undesirable. Ettringite is a complex mineral of hydrated calcium aluminosulfate [2] with the chemical formula $Ca_6[Al(OH)_6]_2(SO_4)_3xH_2O$ where x is around 26. It is usually associated with structural damage and causes reduction of the concrete strength. We have conducted high frequency (0.9 GHz) SAM, SEM, and optical microscopy on a failed concrete sample from a precasting plant which has failed, possibly due to ettringite formation. These analyses were aimed at locating and identifying ettringite and studying its immediate surroundings for changes. At high frequency, SAM [17] is extremely successful in distinguishing between crystalline, “proto-crystalline”, and glassy textures in basalt glasses owing to their large impedance differences. Since a large impedance difference can be expected between various features associated with ettringite formation, we used SAM to map these various features in the failed concrete sample. The acoustic C-scan and SEM images of this sample are shown in Fig. 6. The acoustic image on the left shows a dark colored aggregate in the upper left corner surrounded by cement matrix with colors varying from black to light grey. A bubble is seen in the lower part of the image. The bright area is the void space seen here as filled with epoxy. Between the void space and bubble rim, elongated structures are observed which appear to have grown into the void. This needle-shaped form of ettringite is also clearly seen in the SEM image (Fig. 6b). Apart from their distinct shape, these crystals were identified as ettringite by X-ray microanalyses. Comparing the acoustic and SEM images (Fig. 6), a

circular rim is observed in the acoustical image (Fig. 6a) around the bubble in which the ettringite crystals were found. This rim is not observed in all SEM images. Although the bubble area might be completely filled with ettringite crystals, the impedance change is detectable. Numerous cracks are formed in the SEM analyses.

The needle-shaped crystal form observed in SAM and in SEM, along with EDS of Ca-Al-S ratios, confirms the existence of the ettringite in the sample. The EDS analyses of the various components of Fig. 6a are given in Fig 7. The positions taken were near the reaction rim (columns 1 to 5), at increasing distance from rim, in matrix (columns 6 to 11), and in aggregate (columns 12 to 13). The Ca-Al-S ratios calculated from the these values near the reaction rim compare very well with those for ettringite 3:1:1.5 (column 0 in Fig. 7a). Outside the reaction rim, Ca/Al ratio increases sufficiently. It is around 60 at position 10.

5. Conclusions

We have shown the importance of scanning acoustic microscopy as an important nondestructive in situ technique for analyzing concrete. Applications of SAM shown here are characterizations of aggregate - matrix and bubble - matrix interfaces. In a majority of observations of bubbles, we find a rim of material with different impedance from the surrounding cement matrix. The interface between aggregate and matrix is strongly dependent on the mineralogy of the aggregate grain. In the case of non reactive minerals such as quartz, the grain boundaries are sharp and well defined. The more reactive grains show frayed edges.

We have also compared SAM results with conventional reflected-light optical microscopy and SEM analyses. The major advantage of SAM is that it is an in situ technique with very high resolution. Although SEM has a much higher resolution power than SAM, it produced cracks in all the uncured samples examined here. Reflected-light optical microscopy lacks the image contrast, and transmitted-

light microscopy has the disadvantage of requiring thin sections of the samples. A major, unique advantage of the SAM technique is its capability of penetrating into the material. Acoustic waves reflected from interfaces within the material carry information not only of the surface but also of subsurface characteristics. Thus, subsurface cracks, defects and other zones of weakness that affect the durability and strength of concrete can be mapped nondestructively with high resolution.

Acknowledgements

The authors are thankful to Sidney Mindess for providing the samples for this study. We also thank John Balogh for technical help and Mollie Ebersbach for sample preparation. MP thanks the Stanford Rockphysics and Borehole Project at Stanford University for support during completion of this manuscript. The research was supported by the Office of Advance Research, Federal Highway Administration, under grant number DTFH61-94-X-00020. It is SOEST contribution.

References

1. A. M. NEVILLE, in “Properties of Concrete” (Longman Scientific and Technical, London, 1998).

2. P.K. MEHTA and P.J.M. MONTEIRA, “Concrete. Microstructure, Properties, and Materials” (McGraw_Hill Co., New York, 1993).

3. S. YANG, Z. XU and M. TANG, *Materials and Structures* **31 (**1998) 230.

4. S. DIAMOND and S. MINDESS, *Cement and Concrete Research* **22** (1992) 67.

5. K.K. ALIGIZAKI, B.R. TITTMANN and G.A. GORDON, *Experimental Techniques* **18**, 24, 1994.

6. M. PRASAD, M.H. MANGHNANI and R.A. LIVINGSTON, in The First US-Japan Symposium on Advances in NDT (University of Hawaii, 1996) p. 374.

7. H. UCHIKAWA, in Third CANMET/ACI International Conference, “Advances in Concrete Technology”, Auckland, New Zealand, 1997, edited by V.M. Malhotra (American Concrete Institute, Farmington Hills, 1997) p.109.

8. M.G. ALEXANDER, S. MINDESS, S. DIAMOND and L. QU, *Materials and Structures*, **28,** (1995) 497.

9. M. SANSALONE and N.J. CARINO, in “Handbook on Nondestructive Testing of Concrete”, edited by V.M. Malhotra and N.J. Carino (CRC Press, Boca Raton, 1991) p. 203.

10. M. OHTSU, M. SHIGEISHI and Y. SAKATA, *Ultrasonics* **36** (1998) 187.

11. T. T. WU, and P. L. LIU, *Ultrasonics* **36** (1998) 197.

12. A. BRIGGS, “Acoustic Microscopy” (Clarendon Press, Oxford, 1992).

13. C. J. R. SHEPPARD and T. WILSON, *Appl. Phys. Lett.* **38** (1981) 858.

14. P. ZININ, W. WEISE, O. LOBKIS and S. BOSECK, *Wave Motion* **25** (1997) 213.

16. L.M. BREKHOVSKIKH, in “Waves in Layered Media” (Academic Press, New York, 1980).

17. M. PRASAD and D.J.M. BURKHARD, *Geol. Res. Lett.* (submitted 1998).

Figure Captions

Figure 1. Acoustic (a) and SEM (b) images of concrete sample made with granitic aggregate grains and Portland cement paste. The acoustic image was made at 400 MHz, z=0.

Figure 2. Acoustic images of a concrete mortar sample made with andesitic aggregate grains and with Portland cement paste. The acoustic image was made at 1 GHz, z=0. The box in (a) marks position of the high magnification acoustic image (b).

Figure 3. Acoustical micrographs of a concrete specimen made of andesitic aggregate grains in Portland cement paste with silica fume. (a): frequency 400 MHz; defocus Z = 0 µm. (b): frequency 200 MHz; defocus Z = -100 µm.

Figure 4. (a) reflected light optic, and (b) SEM images of of same area of the specimen shown in Figure 3.The magnification of the optical image is 50*1.25

Figure 5. Bubble in cement mortar; (a) acoustical image made at 400 MHz; (b) SEM image.

Figure 6. Acoustic C-scan (a) and SEM (b) images of the damaged concrete sample from a precasting plant. The image clearly shows a rim around the bubble. Elongated texture within the rim is due to crystals of ettringite. The acoustic image was made at 1 GHz. In SEM image, cracks have been formed due during the process of coating and putting the sample under vacuum.

Fig.7 . EDS analyses of the various components shown in Fig. 7a. Columns 1 to 5 contain data of positions in the reaction rim, columns 6 to 11 at increasing distance from the rim, data in column 12 and 13 was collected from aggregate grains, and column 0 shows EDS analyses of a standard ettringite sample (Ca:Al:S = 3:1:1.5).

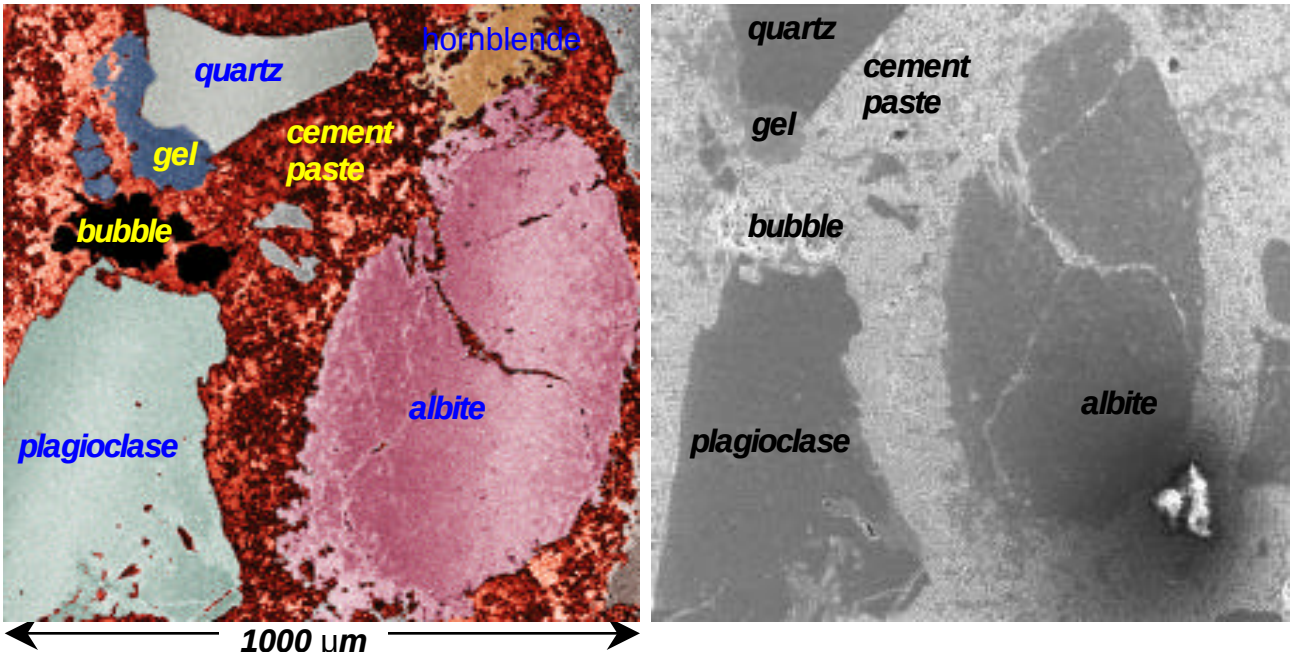

(a) (b)

Figure 1. Acoustic (a) and SEM (b) images of concrete sample made with granitic aggregate grains and Portland cement paste. The acoustic image was made at 400 MHz, z=0.

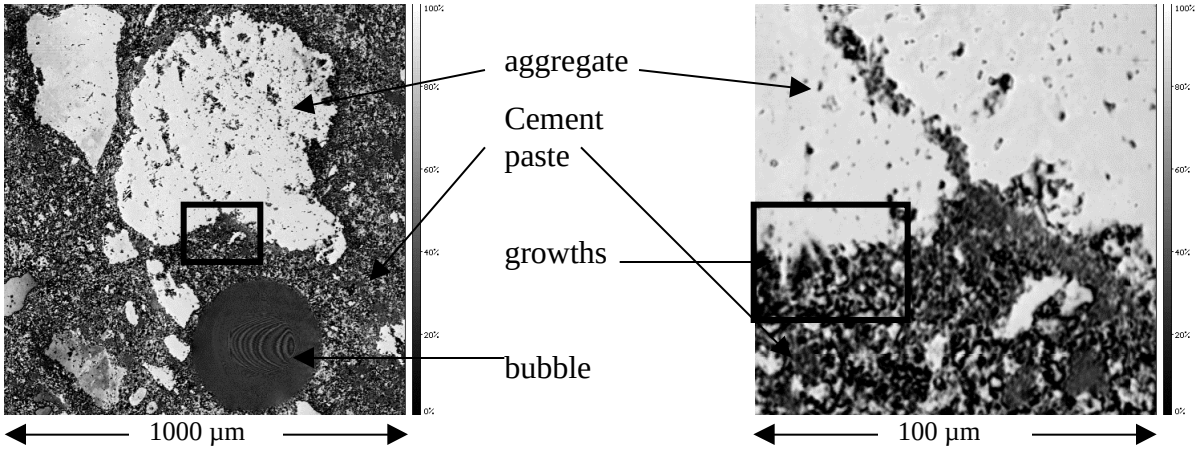

Figure 2. Acoustic images of a concrete mortar sample made with andesitic aggregate grains and with Portland cement paste. The acoustic image was made at 1 GHz, z=0. The box in (a) marks position of the high magnification acoustic image (b).

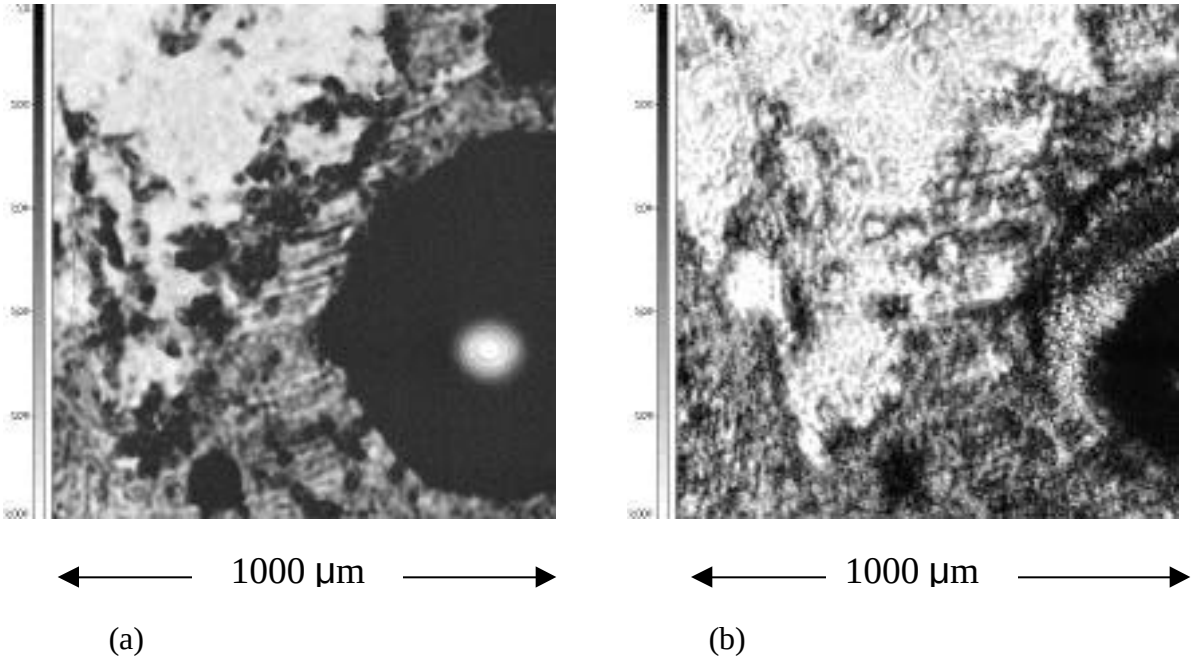

Figure 3. Acoustical micrographs of a concrete specimen made of andesitic aggregate grains in Portland cement paste with silica fume. (a): frequency 400 MHz; defocus Z = 0 µm. (b): frequency 200 MHz; defocus Z = -100 µm.

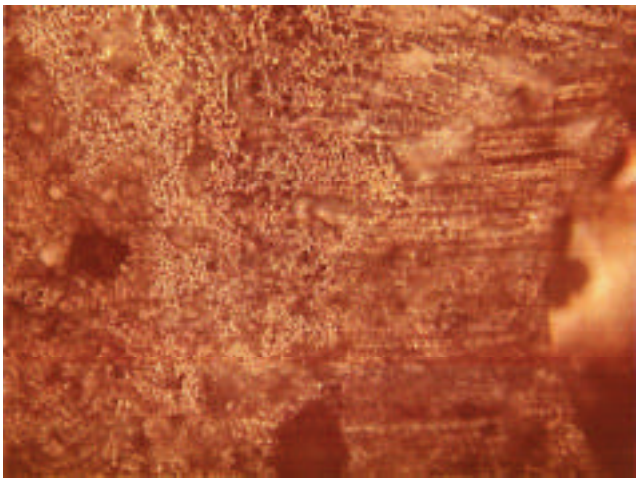

(a)

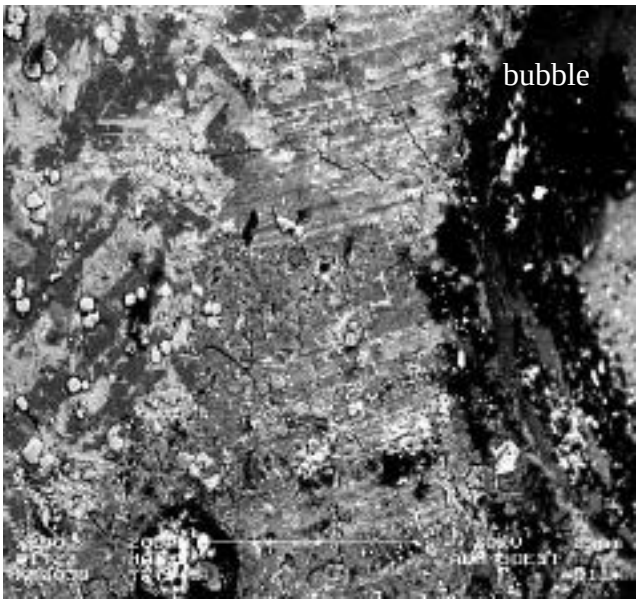

(b)

Figure 4. (a) reflected light optic, and (b) SEM images of of same area of the specimen shown in Figure 3.The magnification of the optical image is 50*1.25

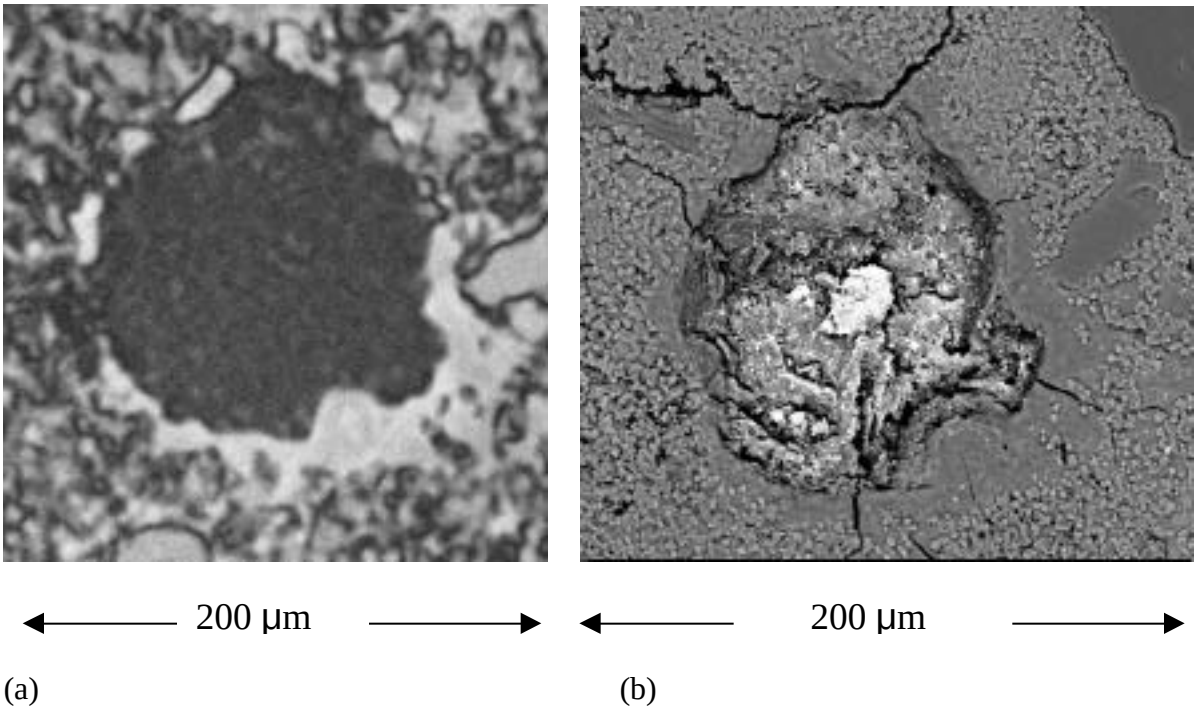

Figure 5. Bubble in cement mortar; (a) acoustical image made at 400 MHz; (b) SEM image.

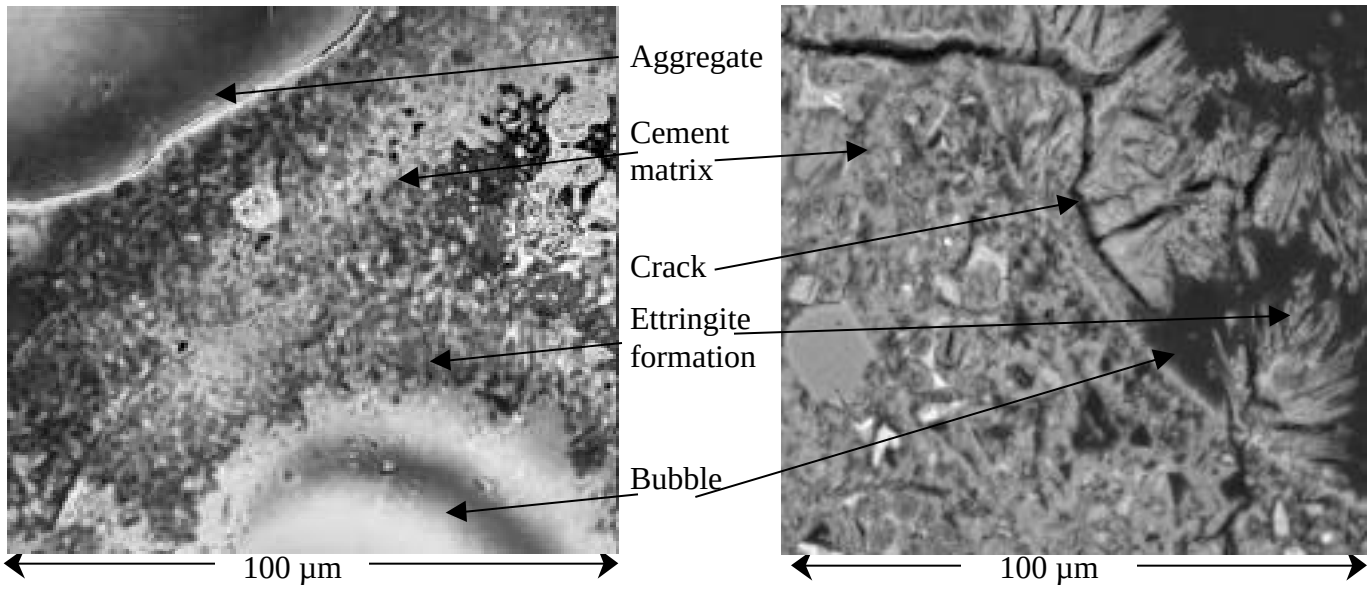

(a) (b)

Figure 6. Acoustic C-scan (a) and SEM (b) images of the damaged concrete sample from a precasting plant. The image clearly shows a rim around the bubble. Elongated texture within the rim is due to crystals of ettringite. The acoustic image was made at 1 GHz. In SEM image, cracks have been formed due during the process of coating and putting the sample under vacuum.

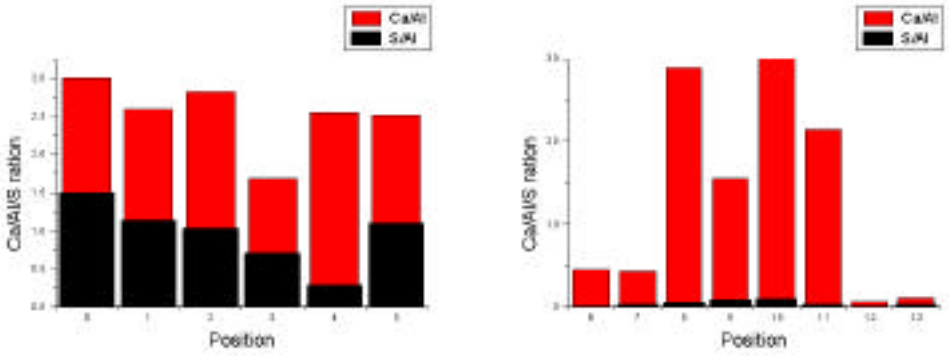

(a) (b)

Fig.7 . EDS analyses of the various components shown in Fig. 7a. Columns 1 to 5 contain data of positions in the reaction rim, columns 6 to 11 at increasing distance from the rim, data in column 12 and 13 was collected from aggregate grains, and column 0 shows EDS analyses of a standard ettringite sample (Ca:Al:S = 3:1:1.5).